First publ. in: Journal of Immunology ; 185 (2010), 9. - pp. 5549-5560

http://dx.doi.org/10.4049/jimmunol.1001517

Reduced Immunoproteasome Formation and Accumulation of Immunoproteasomal Precursors in the Brains of Lymphocytic Choriomeningitis Virus-Infected Mice

Marcel Kremer,* Anja Henn,† Cornelia Kolb,* Michael Basler,*,‡ Jacqueline Moebius,* Benoît Guillaume,§ Marcel Leist,† Benoît J. Van den Eynde,§ and Marcus Groettrup*,‡

Tissue inflammation is accompanied by the cytokine-mediated replacement of constitutive proteasomes by immunoproteasomes that finally leads to an optimized generation of MHC class I restricted epitopes for Ag presentation. The brain is considered an immunoprivileged organ, where both the special anatomy as well as active tolerance mechanisms repress the development of inflammatory responses and help to prevent immunopathological damage. We analyzed the immunoproteasome expression in the brain after an infection with lymphocytic choriomeningitis virus (LCMV) and could show that LCMV-infection of mice leads to the transcriptional induction of inducible proteasome subunits in the brain. However, compared with other organs, i.p. and even intracranial infection with LCMV only led to a faint expression of mature immunoproteasome in the brain and resulted in the accumulation of immunoproteasomal precursors. By immunohistology, we could identify microglia-like cells as the main producers of immunoproteasome, whereas in astrocytes immunoproteasome expression was almost usively restricted to nuclei. Neither the immunoproteasome subunits low molecular mass polypeptide 2 nor multicatalytic endopeptidase complex-like–1 were detected in neurons or oligodendrocytes. In vitro studies of IFN-γ–stimulated primary astrocytes suggested that the observed accumulation of immunoproteasomal precursor complexes takes place in this cell population. Functionally, the lack of immunoproteasomes protracted and lowered the severity of LCMV-induced meningitis in LMP7$^{-/-}$ mice suggesting a contribution of immunoproteasomes in microglia to exacerbate immunopathological damage. We postulate a posttranslationally regulated mechanism that prevents abundant and inappropriate immunoproteasome assembly in the brain and may contribute to the protection of poorly regenerating cells of the CNS from immunopathological destruction.

The proteasome is an ATP-dependent multicatalytic protease complex that is involved in many essential processes within the cytosol and the nucleus. In particular, it is responsible for the generation of peptides presented on MHC class I molecules to CD8$^+$ T cells (1). The eukaryotic 20S proteasome consists of four hetero-heptameric rings, each composed of seven nonidentical α or β-subunits assembled in the order $\alpha_7\beta_7\beta_7\alpha_7$. Of the 14 different proteasomal subunits, only β1, β2, and β5 bear active site threonine residues that function as N-terminal nucleophile hydrolases (2). The three peptidolytically active subunits β1 (Y, δ), β2 (Z, MC14), and β5 (X, MB1) are expressed constitutively in most nonimmunological organs. After stimulation with IFN-γ and/or TNF-α, three inducible subunits β1i (low molecular mass polypeptide 2 [LMP2]), β2i (multicatalytic endopeptidase complex-like–1 [MECL-1]), and β5i (low molecular mass polypeptide 7 [LMP7]) are expressed and incorporated instead of their constitutive counterparts into newly assembled proteasomes, which then are called immunoproteasomes (3–5).

All proteolytically active β-subunits are expressed as inactive precursors bearing N-terminal prosequences, which participate in cooperative proteasome assembly and prevent premature activation. The prosequences are autocatalytically cleaved off during the last step of proteasome assembly rendering the proteasome fully active (6–8). The main function of immunoproteasomes is to produce peptides with basic and hydrophobic C-terminal residues that are better suited as ligands for MHC class I binding. Immunoproteasomes shape the immunodominance of the responding T cell pool by governing the generation as well as the destruction of T cell epitopes (9).

In the human brain, proteasomes are expressed in the cytoplasm, the nuclei, dendrites, axons, and synaptic boutons of a series of different cells including glial cells, pyramidal cells, Purkinje cells, and granular cells in the hippocampus (10, 11). Elevated proteasome activity has been observed after neuronal differentiation, whereas decreased activity and expression are often associated with neurodegenerative disorders and with age leading to protein aggregation, protein oxidation, and age-associated neurodegeneration (12). The expression of immunoproteasome subunits is low in the human brain, and they have been localized in areas such as hippocampus and cerebellum (13). Upregulation of immunoproteasome expression is associated with neuronal differentiation and has been observed during age-progression and neuronal

*Division of Immunology, Department of Biology and †Doerenkamp-Zbinden Chair of in-vitro Toxicology and Biomedicine, Constance University, Konstanz, Germany; ‡Biotechnology Institute Thurgau, University of Constance, Kreuzlingen, Switzerland; and §Ludwig Institute for Cancer Research-Brussels Branch, de Duve Institute, Université catholique de Louvain, Brussels, Belgium

This work was supported by German Research Foundation Grant 1517/4-2.

Address correspondence and reprint requests to Prof. Dr. Marcus Groettrup, Chair of Immunology, Constance University, Universitaetstrasse 10, D-78457 Konstanz, Germany. E-mail address: marcus.groettrup@uni.konstanz.de

The online version of this paper contains supplemental material.

Abbreviations used in this paper: a.u., arbitrary units; CNPase, 2′,3′-cyclic nucleotide 3′-phosphodiesterase; GFAP, glial fibrillary acid protein; Iba-1, ionized calcium-binding adaptor molecule-1; LCMV, lymphocytic choriomeningitis virus; LMP2, low molecular mass polypeptide 2; LMP7, low molecular mass polypeptide 7; m, mouse; MECL-1, multicatalytic endopeptidase complex-like–1; NEPHGE, nonequilibrium pH gradient electrophoresis; PFA, paraformaldehyde.

disorders such as Huntington's disease and Alzheimer's disease (10, 14). In primary mouse microglia cultures, the expression of immunoproteasome subunits could be induced upon stimulation with IFN-γ (15). Other than these in vitro data, little is known about the in vivo expression of immunoproteasome in the murine brain under normal and inflammatory conditions.

In this study, we analyzed the formation of immunoproteasome in the murine brain after lymphocytic choriomeningitis virus (LCMV) infection. Compared with that in other organs, the gross immunoproteasome induction in the brain is very low even after intracranial infection. Whereas microglia readily expressed mature immunoproteasome, no immunoproteasome formation could be detected in neurons and oligodendrocytes. In astrocytes, immunoproteasome expression was low and confined to the nucleus. An accumulation of unprocessed immunoproteasomal precursors in primary astrocytes in vitro may correspond with the observed accumulation of immunoproteasomal precursors in LCMV-infected mouse brain in vivo. The apparent attenuation of immunoproteasome formation may contribute to the immune privilege of the CNS.

Materials and Methods

Animals

C57BL/6 mice (H-2^b) mice were originally obtained from Charles River Laboratories, Kisslegg, Germany. BALB/c (H-2^d) mice were obtained from the animal facility of the University of Constance and kept in a specific pathogen-free facility. MECL-$1^{-/-}$ mice (16), $LMP2^{-/-}$ mice (17), and $LMP7^{-/-}$ mice (18), back-crossed to C57BL/6 background for at least 10 generations, were a kind gift of Prof. Dr. John Monaco (Department of Molecular Genetics, College of Medicine, University of Cincinnati, Cincinnati, OH). Homozygous MECL-$1^{-/-}$/$LMP7^{-/-}$ mice (L7M mice) or MECL-$1^{-/-}$/$LMP2^{-/-}$ mice (L2M mice) were obtained by interbreeding the respective single gene targeted mice. For the experiments, 8- to 12-wk-old and sex-matched mice were used. Animal experiments were approved by the review board of Regierungspräsidium Freiburg.

Virus

LCMV-WE was originally obtained from F. Lehmann-Grube (Hamburg, Germany) and propagated on the fibroblast line L929. Mice were infected with either 200 PFU LCMV-WE i.v. and 30 PFU intracranially or simultaneously with 30 PFU intracranially and 10^5 PFU i.p.

Antibodies

The monoclonal mouse Ab α-p27, clone IB5, recognizes the α1-subunit iota of the proteasome and was obtained from Prof. Dr. Klaus Scherrer (Institut Jacques Monod, Paris, France). Polyclonal rabbit antisera were raised against epitopes of MECL-1 (β2i) and LMP2 (β1i), which are accessible on the outer surface of the immunoproteasome (B. Guillaume, J. Chapiro, V. Stroobant, D. Colau, B. Van Holle, G. Parvizi, M.P. Bousquet-Dubouch, I. Théate, N. Parmentier, and B.J. Van den Eynde, submitted for publication). They were affinity purified and used in a 1:10000 dilution for Western blot analysis or in a 1:2000 dilution for immunohistochemistry. Polyclonal Ab recognizing LMP7 was a rabbit antiserum raised against the keyhole limpet hemocyanin-coupled peptide SDVSDLLYKYGEAAL of mouse LMP7 (mLMP7) (19). As secondary Abs, polyclonal HRP-coupled goat anti-mouse IgG (1:1000; product No. P0447; Dako, Hamburg, Germany) or HRP-coupled swine anti-rabbit IgG (1:2000; product No. P0399; Dako) were used for immunoblotting. For immunohistochemistry, we used the primary Abs goat anti-ionized calcium-binding adaptor molecule-1 (Iba-1) (1:100; product No. ab5076; Abcam, Berlin, Germany) for the detection of microglia, mouse antiglial fibrillary acid protein (GFAP) (1:1000; product No. G6171; Sigma-Aldrich, Munich, Germany) for the detection of astrocytes, mouse anti-NeuN (1:200; product No. MAB377; Chemicon, Hofheim, Germany) for the detection of neurons, mouse anti-2′,3′-cyclic nucleotide 3′-phosphodiesterase (CNPase) (1:1000; product No. C5922; Sigma-Aldrich) for the detection of oligodendrocytes, rat anti-VL4 (undiluted rat hybridoma supernatant) for the detection of LCMV, and rat anti-CD3 (1:200; product No. MCA1477; Serotec, Düsseldorf, Germany) for the detection of infiltrating T cells. Visualization was performed using cy3-conjugated donkey anti-rabbit IgG (1:1000; product No. 711-166-152; Jackson ImmunoResearch, Suffolk, U.K.), cy3-conjugated donkey anti-rat IgG (1:1000; product No. 712-166-150; Jackson ImmunoResearch), Alexa 488-conjugated donkey anti-goat IgG (1:1000; product No. A11055; Invitrogen, Karsruhe, Germany), and Alexa 488-conjugated goat anti-mouse IgG (1:1000; product No. A11017; Invitrogen). For immunohistochemistry, all Abs were diluted in PBS containing 0.1% Tween 20 (product No. P1379; Sigma-Aldrich) and 1% BSA (Sigma-Aldrich). Cell nuclei were stained using 4′,6′-diamidino-2-phenylindole dihydrochloride (1:1000; product No. 32670; Sigma-Aldrich).

Purification of 20S proteasomes, proteasome activity assays, nonequilibrium pH gradient electrophoresis/SDS-PAGE, and Western blotting

The purification and activity assay of 20S proteasomes, nonequilibrium pH gradient electrophoresis (NEPHGE)/SDS-PAGE, and Western blot analysis was exactly performed as previously described (19).

Sucrose gradient density centrifugation

One hundred milligrams of liver or brain tissue were lysed in buffer II (0.1 M KCl, 5 mM $MgCl_2$, 10 mM HEPES, pH 7.2, 0.1% Triton X-100) using a Dounce homogenizer. After sonification (5 cycles of 20 s; 60% intensity), the homogenate was centrifuged at 20,000 × *g* for 30 min at 4°C. The supernatant was loaded onto a gradient of 15–40% sucrose in 0.1 M KCl buffer and centrifuged at 40,000 rpm for 16 h at 4°C in a Beckman-Coulter (Krefeld, Germany) SW40Ti rotor. Afterward, fractions of 600 μl were drawn, and proteasome activity was determined. Two hundred fifty microliters of each fraction were then precipitated according to Wessel and Flügge (20). After a drying period, pellets were dissolved in 2% SDS and separated by SDS-PAGE. Proteasomal subunits were detected by Western blot analysis.

Quantitative RT-PCR

RNA was prepared from brain and liver samples or T2 clones, respectively, using the NucleoSpin RNA II Kit (product No. 740955250; Machery-Nagel, Düren, Germany) according to the manufacturer's manual. For the synthesis of single-stranded cDNA from pure total RNA, the ReverseTranscription System Kit (product No.A3500; Promega, Mannheim, Germany) was used. To determine relative gene expression, the LightCycler Fast Start DNA Master SYBR Green I Kit (product No. 12239264001; Roche, Grenzach-Wyhlen, Germany) was used in conjunction with the LightCycler Instrument (Roche) and the LightCycler Software Version 3.5 (Roche). Concerning the determination of relative IFN-γ expression, the TaqMan Master Kit (product No. 04535286001; Roche) was used in combination with an IFN-γ–specific probe (product No. 04686942001; Roche).

Sense and antisense primers used for the PCR amplification were as follows: mouse (m)IFN-γ: 5′-ATC TGG AGG AAC TGG CAA AA-3′ and 5′-TTC AAG ACT TCA AAG AGT CTG AGG-3′ (annealing temperature = 60°C); mHPRT: 5′-TGG ACA GGA CTG AAA GAC TTG-3′ and 5′-CCA GCA GGT CAG CAA AGA ACT TA-3′ (annealing temperature = 59°C); mMECL-1: 5′-CGT CTG CCC TTT ACT GC-3′ and 5′-CCA CTT CAT TCC ACC TCC-3′ (annealing temperature = 62°C); mLMP2: 5′-TCC ACA CCG GGA CAA CC-3′ and 5′-CCA GCC AGC TAC TAT GAG ATG C-3′ (annealing temperature = 62°C); mLMP7: 5′-CTC CGT GTC TGC AGC ATC C-3′ and 5′-TCC ACT TTC ACC CAA CCG TC-3′ (annealing temperature = 60°C). The runs were programmed as follows: denaturation for 10 min at 95°C, amplification (35 cycles [40 cycles for mHPRT] with reading of the fluorescence at the end of each cycle) for 10 s at 95°C, 30 s at annealing temperature, 20 s at 72°C; and analysis of the products (reading of the fluorescence in a continuous mode) for 0 s at 95°C, 62°C to 95°C transition with 0.1°C increment/second. For the detection of IFN-γ expression, we used the TaqMan Master Kit (product No. 04535286001; Roche) in combination with an IFN-γ–specific probe (product No. 04686942001; Roche). This run was programmed as follows: denaturation for 10 min at 95°C and amplification (48 cycles with reading of the fluorescence at the end of each cycle) for 10 s at 95°C, 30 s at annealing temperature, and 1 s at 72°C. The specificity of the amplification was verified by melting curve analysis (95°C for 0 s; 65°C for 15 s, 95° for 0 s with a temperature transition rate of 0.1°C/s in a continuous acquisition mode) or in case of IFN-γ by gel analysis of the amplified product. Relative gene expression was normalized to mHPRT mRNA content and evaluated according to the Pfaffl method using the Excel-based software tool REST (21).

Immunohistochemistry

Mice were either infected with 30 PFU LCMV-WE intracranially or coinfected with 30 PFU LCMV-WE intracranially and 10^5 PFU i.p. On day 7 after intracranial infection or on day 10 after combined intracranial and i.p. infection, respectively, mice were anesthetized and transcardially

perfused with 20 ml 4% paraformaldehyde (PFA)/PBS. Brains were prepared and postfixed in 4% PFA/PBS at 4°C overnight. For Ag retrieval, organs were subsequently immersed in Ag retrieval solution (10 mM sodium citrate buffer, 0.05% Tween 20, pH 6) at 4°C overnight and further boiled for 4 min in fresh retrieval solution before transfer to 30% sucrose/PBS and immersion overnight for cryopreservation. Brain samples were subsequently embedded in Tissue-Tec OCT (Sakura, Düsseldorf, Germany), snap-cap frozen in liquid nitrogen, and stored at –80°C until use. Cryostat sections (18 μm) were mounted on Superfrost plus slides (Thermo Scientific, Karlsruhe, Germany), air dried, and circled with a liquid blocker. After preincubation in 50 mM NH_4Cl/PBS for 15 min, sections were permeabilized with 0.1% Nonidet P-40 (NP-40)/PBS for 30 min. To reduce unspecific binding, sections were further incubated for 1 h at room temperature in 0.2% BSA/PBS plus 2% normal donkey serum (Sigma-Aldrich). After blocking, incubations with primary Abs were performed in 0.2% BSA/PBS overnight at 4°C with the following dilutions: rabbit anti-LMP2 (1:2000), rabbit anti-MECL-1 (1:2000), goat anti–Iba-1 (1:100), mouse anti-GFAP (1:1000), mouse anti-NeuN (1:200), and mouse anti-CNPase (1:1000). Slides were each washed 3 times in PBS for 5 min before they were incubated for 2 h at room temperature with cocktails of the secondary Abs containing anti-rabbit IgG-cy3 (1:1000), anti-goat IgG-Alexa 488 (1:1000), and/or anti-mouse IgG-Alexa 488 (1:1000), respectively, diluted in PBS and supplemented with DAPI (1:1000).

For the detection of LCMV as well as the detection of T cell infiltration, organs were isolated and directly embedded in Tissue-Tec OCT (Sakura). Cryostat sections (10–20 μm) were mounted on Superfrost plus slides (Thermo Scientific), air dried, and circled with a liquid blocker. For the VL4 staining, sections were fixed for 10 min in 4% PFA, incubated in 50 mM NH_4Cl/PBS for 15 min, and further permeabilized with 0.1% NP-40/PBS for 30 min. After blocking in 0.2% BSA/PBS for 1 h at room temperature, sections were incubated overnight at 4°C with the supernatant of a VL4 hybridoma followed by staining with a secondary anti–rat-cy3 IgG (1:1000) diluted in PBS. For CD3 staining, sections were fixed for 15 min in cold 100% ethanol, air dried, and further washed twice for 5 min in PBS supplemented with 0.1% Tween 20 (Sigma-Aldrich). For Ag retrieval, sections were further boiled in 0.2% citric acid (pH 6) for 30 min in a microwave oven and kept at room temperature for a further 30 min. Sections were subsequently washed twice in PBS and circled with a liquid blocker. Unspecific binding was blocked by incubation in PBS/0.1% Tween 20/1% BSA for 10 min. Detection of infiltrating T cells was performed by incubation of the sections with the primary Ab rat anti-human CD3 (diluted 1:200 in PBS/0.1% Tween/1% BSA) at 4°C overnight. Visualization was performed using a secondary cy3-coupled anti-rat IgG (1:1000). After washing, slides were always mounted in Moviol (Calbiochem, Bad Soden, Germany) and analyzed with a Zeiss Axioplan (Göttingen, Germany) microscope using the AxioVision Rel 4.6 and the ImageJ software.

Isolation of CD11b$^+$ cells

For the isolation of CD11b$^+$ cells, single-cell suspensions were generated according to the manufacturer's instructions from whole BALB/c brains using a commercially available neuronal dissociation kit (product No. 130093231; Miltenyi, Bergisch Gladbach, Germany). CD11b$^+$ cells were isolated out of these suspensions by the MACS technology according to the manufacturer's instructions using 15 μl CD11b microbeads (product No. 130049601; Miltenyi) per brain. To increase the purity, eluted cells were administered to a second column and the purification procedure repeated. Purity of the isolated CD11b$^+$ and CD11b$^-$ (flow-through) fractions was subsequently checked by flow cytometry and reached a purity of 75–90%. An aliquot of 50 μl of each fraction was incubated for 20 min at 4°C with an FITC-conjugated mouse anti-CD11b IgG (dilution 1:150 in FACS buffer [PBS supplemented with 2 mM EDTA, 2% FCS, 2 mM sodium acid]; product No. MCA74FA; AbD Serotec). After two washing steps in 150 μl FACS buffer, cells were dissolved in 200 μl FACS buffer and analyzed by flow cytometry using a FACScan flow cytometer (BD, Heidelberg, Germany) and the FloJo software (Tree Star, Olten, Switzerland). Isolated fractions were subsequently used for western blot analysis.

Preparation of primary astrocytes and astrocyte cell lines

Primary cortical astrocytes were prepared from 1- to 2-d-old BALB/c mice according to Falsig et al. (22). Immortalized astrocytes were originally generated in the laboratory of Klaus Pfizenmaier (IZI, University of Stuttgart, Germany) based on a protocol by Frisa et al. (23). Cells were either left untreated or stimulated for 72 h in the presence of 20 ng/ml IFN-γ and further used for Western blot analysis.

Disease score

C57BL/6 and LMP7$^{-/-}$ mice were intracranially infected with 30 PFU LCMV-WE. From day 5 to day 7 postinfection, the degree of disease was regularly scored in a blinded manner according to Langford et al. (24) with minor modifications. The evaluated categories 1) orbital tightening, 2) nose bulge, 3) ear position, 4) hunchback, and 5) locomotion constraint were separately graded as follows: 0, not present; 1, moderate; and 2, severe. The sum of the scores for each of the five categories yielded the final disease score.

Results

Extensive replacement of constitutive proteasomes by immunoproteasomes in most organs after LCMV infection

After a viral infection, IFN-γ is released by T cells and NK cells and leads to the induction of immunoproteasomes. To investigate the extent of immunoproteasome induction, the subunit composition of proteasomes was analyzed in different organs from noninfected and virus-infected BALB/c mice by two-dimensional gel electrophoresis. Mice were infected with LCMV-WE i.v., and 8 d later, 20S proteasomes were isolated from liver, heart, lung, kidney, colon, intestine, and spleen and analyzed by NEPHGE/SDS-PAGE. In an uninfected state, all nonimmunological organs mainly contained constitutive proteasome indicated by the predominant presence of the constitutive subunits δ (β1) and MB1 (β5). Also, marginal amounts of the corresponding immunoproteasome subunits LMP2 (β1i) and LMP7 (β5i) could be observed under noninflammatory conditions in these organs. A higher basal immunoproteasome expression was observed in spleen, lung, colon, and intestine. After infection with LCMV, LMP2 and LMP7 were strongly upregulated, whereas their constitutive counterparts δ and MB1 had either disappeared completely or were significantly decreased (Fig. 1).

Very low expression of immunoproteasome in the brains of LCMV-infected mice

Next we analyzed the proteasome subunit composition of the brain. To set an acute infection in the brain, BALB/c mice were intracranially infected with 30 PFU LCMV-WE. In contrast with an i.v. infection, an intracranial infection with LCMV avoids a preterm clearance of the virus in the periphery and guarantees a local inflammation of the brain, which leads to a lethal choriomeningitis on day 7 postinfection. At the first signs of disease, mice were euthanized, and proteasomes were isolated from the brain and analyzed by two-dimensional gel electrophoresis (Fig. 2*A*). In contrast with other organs (Fig. 1), there was no expression of immunoproteasomes in the brain of uninfected mice or after i.v. infection with LCMV-WE. Intracranial infection with LCMV merely resulted in a slight induction of LMP2 and LMP7 on day 7 postinfection.

To exclude that the low degree of immunoproteasome formation is a consequence of the dramatic course of disease and based on the short time period available for transcription, translation, and/or assembly of newly synthesized proteasomes, we changed our infection protocol to allow a more moderate course of meningitis resulting in survival and eventual recovery of the mice. To this end, mice were coinfected with 10^5 PFU LCMV-WE i.p. and 30 PFU LCMV-WE intracranially. This protocol leads to more rapid T cell priming and induction of an LCMV-specific CTL response in the periphery, which reduces the viral load and results in a diminished CTL-mediated immunopathology (25). After coinfection, the mice showed typical symptoms of ongoing inflammation like bristled fur and an apathetic behavior, but, compared with mice that were only infected intracranially, they showed a moderate course of disease and survived day 7, sometimes recovering completely. The

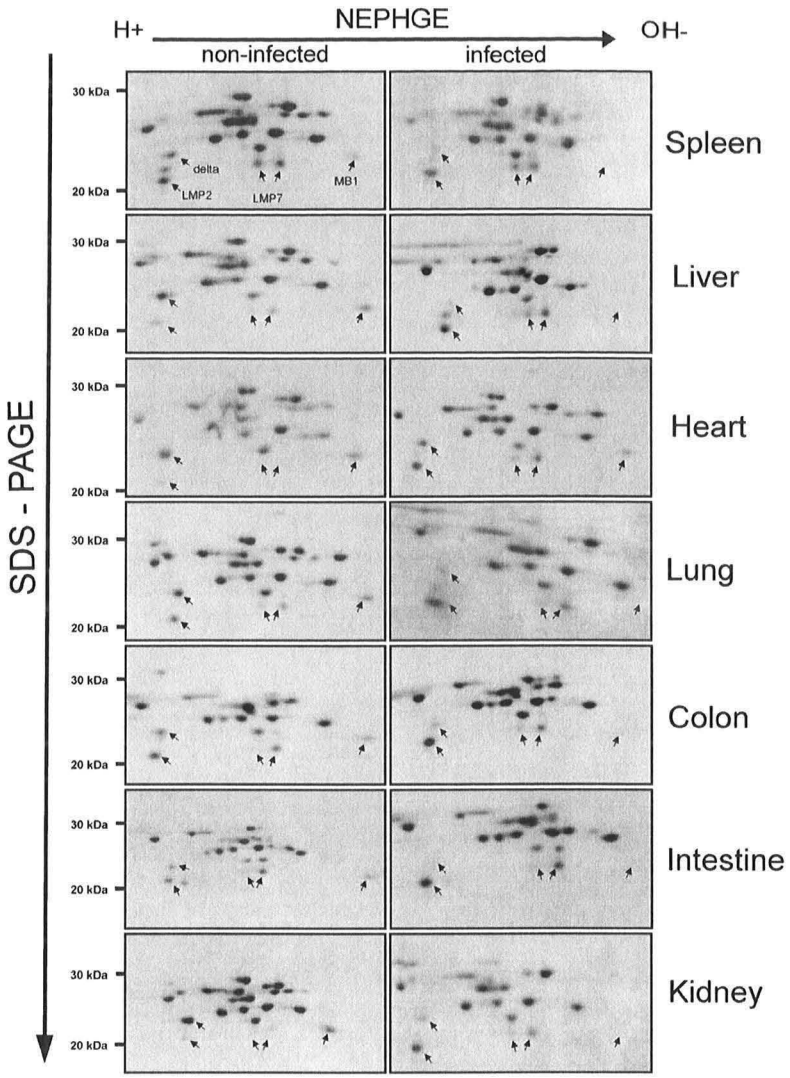

FIGURE 1. Composition of isolated 20S proteasomes in different organs analyzed by two-dimensional gel electrophoresis. The 20S proteasomes were purified from different organs of naive (*left panels*) and i.v. LCMV-infected (*right panels*) BALB/c mice on day 8 postinfection. The subunit pattern was analyzed by Coomassie blue-stained NEPHGE/SDS-PAGE. Black arrows indicate the immunoproteasome subunits LMP2 (β1i) and LMP7 (β5i) as well as their constitutive counterparts δ (β1) and MB1 (β5). The experiments were performed twice with similar outcome.

coinfection protocol failed to induce substantial levels of immunoproteasomes up to day 10 postinfection when compared with other organs (Fig. 1; for a densitometric analysis of LMP2, δ, LMP7, and MB1 spots in liver and brain, see Fig. 2*B*). We conclude that the failure to detect immunoproteasome formation in the brain cannot be attributed to an early death after intracranial LCMV infection.

mRNA expression of IFN-γ and immunoproteasome subunits in livers and brains of LCMV-infected mice

To investigate the molecular basis of attenuated immunoproteasome formation in the brain, we analyzed the mRNA expression of IFN-γ and immunoproteasome subunits by real-time reverse transcription-PCR. Mice were infected either with 200 PFU LCMV-WE i.v., with 30 PFU intracranially, or simultaneously with 10^5 PFU i.p. and 30 PFU intracranially. Either on day 7 (single i.v. or i.p. infection) or on day 10 postinfection (combined i.v. and i.p. infection), RNA was isolated from liver and brain, and the mRNA expression for IFN-γ, MECL-1, LMP2, and LMP7 was quantified. After i.v. infection, we observed an up to 60-fold induction of IFN-γ in the liver on day 6 postinfection, which decreased quite rapidly to a less than 20-fold induction on day 8 (Fig. 3*A*). Immunoproteasome subunits were upregulated by 4- to 10-fold on day 4. This level remained stable until day 6 and then decreased to a lower magnitude on day 8. Surprisingly, this induction had occurred on day 4, when there was still no IFN-γ expression detectable. Probably, this can be attributed to other proinflammatory cytokines, such as TNF-α and type I IFNs (IFN-α, IFN-β), which are known to induce immunoproteasome expression as well (26). Intracranial infection as well as the coinfection protocol yielded a similar kinetic in the liver, although—except for IFN-γ and MECL-1 in the coinfection model—the relative induction was significantly decreased compared with that for i.v. infection. Intravenous LCMV infection failed to induce high mRNA levels for IFN-γ and the immunoproteasome subunits in the brain probably because the virus was cleared before it could cause a meningitis (Fig. 3*B*).

In contrast, after coinfection and intracranial infection, we saw a fulminant 200- to 400-fold upregulation of IFN-γ mRNA in the brain, probably due to the infiltration of mononuclear cells (27). Whereas IFN-γ expression after intracranial infection was strongly induced on day 6 and further increased until day 7, upregulation of this cytokine in coinfected mice peaked on day 6 and declined thereafter. For the mRNA expression of immunoproteasome subunits in the brain of intracranially infected mice, we observed a steady increase up to day 7 with an up to 6-fold induction for MECL-1, up to 120-fold induction for LMP2, and up to 8-fold induction for LMP7. The relatively stronger induction of

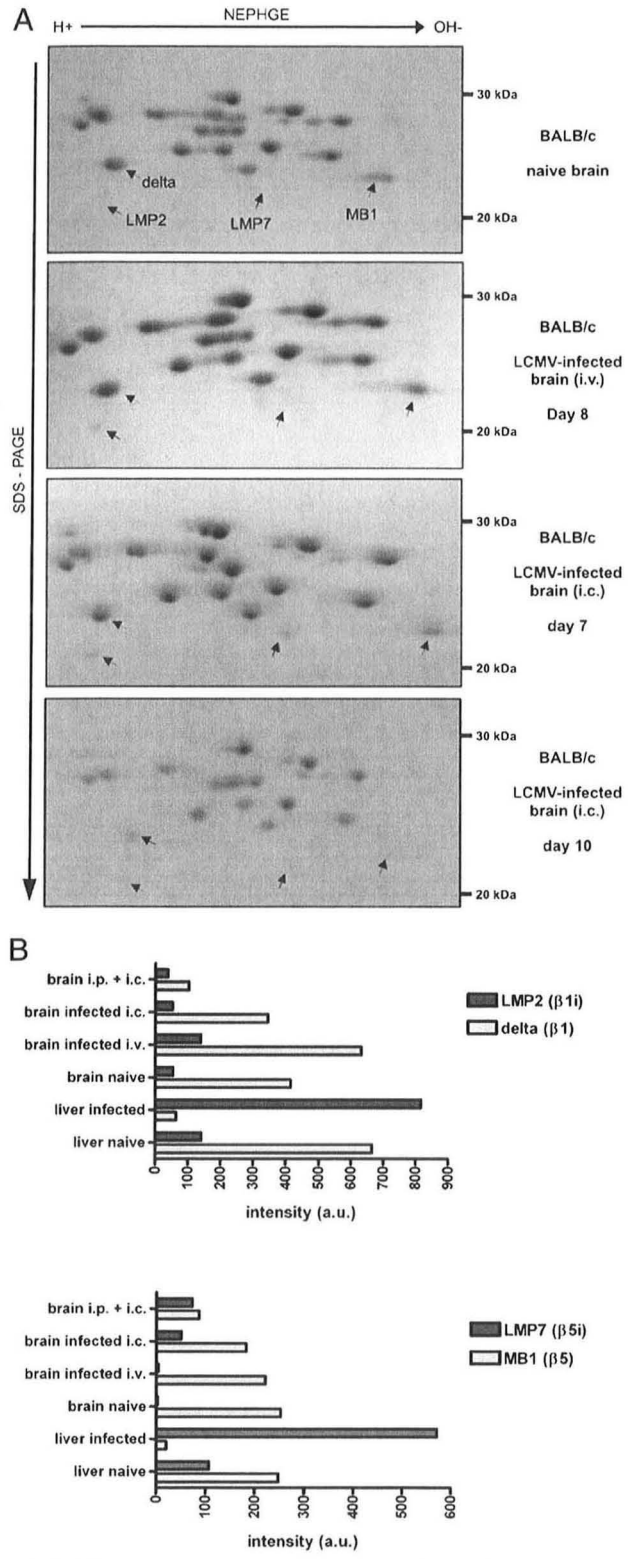

FIGURE 2. Proteasome composition in the brain of naive and LCMV-infected BALB/c mice. *A*, Mice were either left untreated, infected with 200 PFU LCMV i.v. and analyzed on day 8 postinfection, or infected with 30 PFU LCMV intracranially and analyzed on day 7, or coinfected with 30 PFU LCMV intracranially and 10^5 PFU i.p. followed by analysis on day 10. Proteasomes were isolated from the brain as indicated, and their subunit composition was analyzed by NEPHGE/SDS-PAGE followed by staining with Coomassie blue. The experiments were performed twice and yielded similar results. *B*, The densities of spots for LMP2 (β1i), δ (β1), LMP7 (β5i), and MB1 (β5) were assessed in the two-dimensional gels shown in Fig. 1 (liver) and this figure (brain), and the results (in a.u.) were charted as shown. a.u., arbitrary units.

LMP2 compared with that of LMP7 and MECL-1 was probably due to extremely low LMP2 expression levels in the uninfected brain. Also, the coinfection protocol resulted in a substantial mRNA induction for MECL-1, LMP2, and LMP7 throughout day 4 to day 10 after which mice were sacrificed for the analysis of proteasome subunit composition (Fig. 2).

Taken together, these data indicate that after intracranial infection with LCMV, the low level of immunoproteasome cannot be attributed to a lack of time for the induction of immunoproteasome. Even in the coinfection model, only minimal immunoproteasome formation could be detected on two-dimensional gels, whereas the same period of immunoproteasome synthesis in the liver of i.v.-infected mice led to an extensive replacement of constitutive proteasomes by immunoproteasomes (Fig. 2*B*) (19).

Expression of immunoproteasome subunits in livers and brains of LCMV-infected mice on protein level

After induction by IFN-γ, the immunoproteasome subunits MECL-1, LMP2, and LMP7 are synthesized as N-terminal extended precursor subunits, which then are autocatalytically processed during the assembly of the immunoproteasome (6, 7). To investigate further the poor immunoproteasome formation in the brain, the expression of its subunits was analyzed on the protein level by Western blot analysis. Mice were infected either with 200 PFU i.v. or with 30 PFU intracranially. On day 8 postinfection, organs were recovered and analyzed by Western blot using Abs specific for MECL-1, LMP2, and LMP7 (Fig. 4). Positive controls were 20S immunoproteasomes purified from the liver of LCMV-infected mice. As a control for equal proteasome loading, we monitored the α-type subunit iota (α1), which is part of both the constitutive proteasome and the immunoproteasome. Mature MECL-1 with a molecular mass of 25 kDa could be observed in liver and brain of wild-type mice. No MECL-1 was detected in LMP7 and MECL-1 double knockout mice (L7M) as well as in LMP2 knockout mice due to the requirement of LMP2 for the incorporation of MECL-1 (28). Mature LMP2 with a molecular mass of 21 kDa and mature LMP7 (23 kDa) were expressed in all samples except for the ones from the corresponding knockout mice. In the LMP2 blot, an additional band of ~23 kDa appeared in brain samples of intracranially LCMV-infected BALB/c mice. Such a band was also prominent in the liver sample of the L7M double knockout mouse, which is expected to represent the LMP2 precursor as it accumulated in the absence of LMP7 and was absent in $LMP2^{-/-}$ mice (8). It appears that the reduced immunoproteasome formation in the brain of LCMV-infected BALB/c might be due to an assembly defect.

Accumulation of immunoproteasome precursors in the brains of LCMV-infected BALB/c mice

To investigate further whether LMP2 precursors accumulate in brain, we performed sucrose gradient centrifugation. BALB/c mice as well as $MECL\text{-}1^{-/-}/LMP2^{-/-}$ double knockout mice were infected i.v. or intracranially with LCMV-WE. On day 8 and day 7 postinfection, liver and brain lysates, respectively, were recovered and total lysates subjected to density gradient centrifugation, and fractions were analyzed by Western blotting. In the liver of LCMV-infected mice (Fig. 5*A*), mature immunoproteasomes containing processed MECL-1 (25 kDa), LMP2 (21 kDa), and LMP7 (23 kDa) were found in the fractions 9–14. In the brain samples

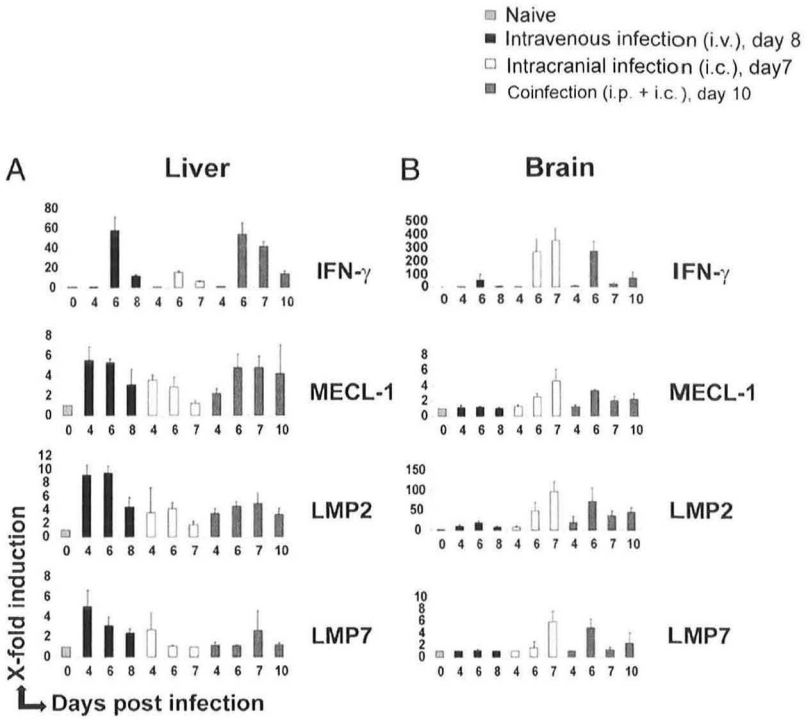

FIGURE 3. mRNA levels of immunoproteasome subunits in the liver and the brain of naive and LCMV-WE–infected BALB/c mice. Mice were either left untreated, intravenously infected with 200 PFU LCMV-WE i.v., 30 PFU intracranially (i.c.), or coinfected with 30 PFU intracranially and 10^5 PFU i.p. At indicated time points postinfection, RNA was isolated from total liver or brain, transcribed into cDNA, and the gene induction of IFN-γ, MECL-1, LMP2, and LMP7 was analyzed by RT-PCR. *A*, mRNA induction in the liver. *B*, mRNA induction in the brain. All samples were normalized to HPRT expression. The experiments were performed three times with similar outcome; shown are the means of three experiments ± SEM.

(Fig. 5*B*), LMP2 and MECL-1 blots showed additional bands of 23 kDa and 29, which correspond with the expected sizes of their respective unprocessed precursors. The fact that these additional bands are missing in immunoblots of MECL-$1^{-/-}$/$LMP2^{-/-}$ mice (Fig. 5*C*) as well as their presence in fractions of lower density (Fig. 5*B*) strongly support that they represent unprocessed immunoproteasome subunits, which are assembled in 16S precursor complexes. A similar accumulation of LMP2 and MECL-1 precursors was not found in the livers of LCMV-infected mice even upon overexposure (Fig. 5*A* and data not shown) consistent with a rapid conversion of precursor complexes into mature proteasomes. Taken together, these data suggest that an impaired proteasome assembly contributes to the observed incomplete replacement of constitutive proteasome by immunoproteasome in the brain.

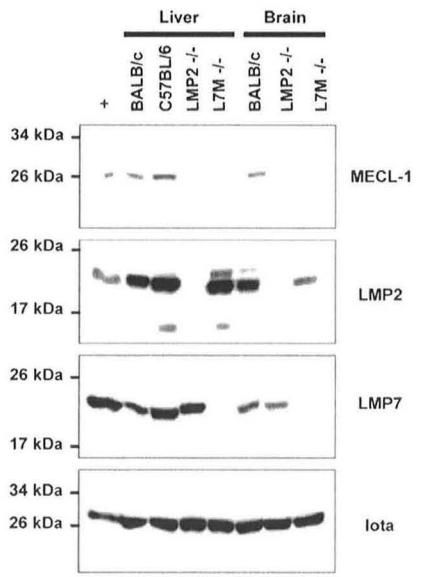

FIGURE 4. Western blot analysis of immunoproteasome expression in liver and brain of LCMV-WE–infected mice. Immunoproteasome expression was analyzed by Western blot in total lysates of intravenously infected liver and intracranially infected brain of wild-type, $LMP2^{-/-}$, or $LMP7^{-/-}$/MECL-$1^{-/-}$ ($L7M^{-/-}$) double knockout mice. As a positive control (+), purified immunoproteasome from LCMV-WE–infected BALB/c liver was used. Note the emergence of an additional band of ~23 kDa in the LMP2 blot of brain tissue, which represents unprocessed LMP2 precursor. A representative experiment out of three performed is shown.

Localization of LMP2 and MECL-1 in the brains of intracranially LCMV-infected BALB/c mice

To gain further insight into immunoproteasome expression in the brain after LCMV infection, we pursued a histologic approach and analyzed brain inflammation by immunofluorescence microscopy. Sections from the brain of LCMV-infected BALB/c mice and naive control mice were stained with DAPI and the LCMV nucleoprotein-specific mAb VL4. In accordance with a previous study (29), viral infection was prominent in the meninges, the ependymal cells of the ventricles, and the choroid plexus as well as in the regions around the ventricles on day 7 after intracranial LCMV infection (data not shown). Because LCMV is a noncytopathic virus, the damage induced in the CNS is not caused by the virus, but is rather a result of the subsequent immune response and caused by infiltrating T cells. Whereas we observed no T cell infiltration in the brain of naive control mice, T cell infiltration in the infected brains strongly correlated with the sites of LCMV infection (data not shown).

To identify cell types within the brain by immunofluorescence histology that express immunoproteasome and may account for the accumulation of immunoproteasomal precursors, we used newly generated polyclonal Abs specific for MECL-1 and LMP2, which bind to epitopes predicted to lie on the outer surface of immunoproteasomes (B. Guillaume et al., submitted for publication). The specificity of these Abs was verified extensively in intracranially LCMV-infected wild-type and MECL-$1^{-/-}$/$LMP2^{-/-}$ double-knockout mice (Supplemental Figs. 1, 2); stainings with the second-stage reagents alone also showed no fluorescence above background (data not shown). The highest LMP2 and MECL-1

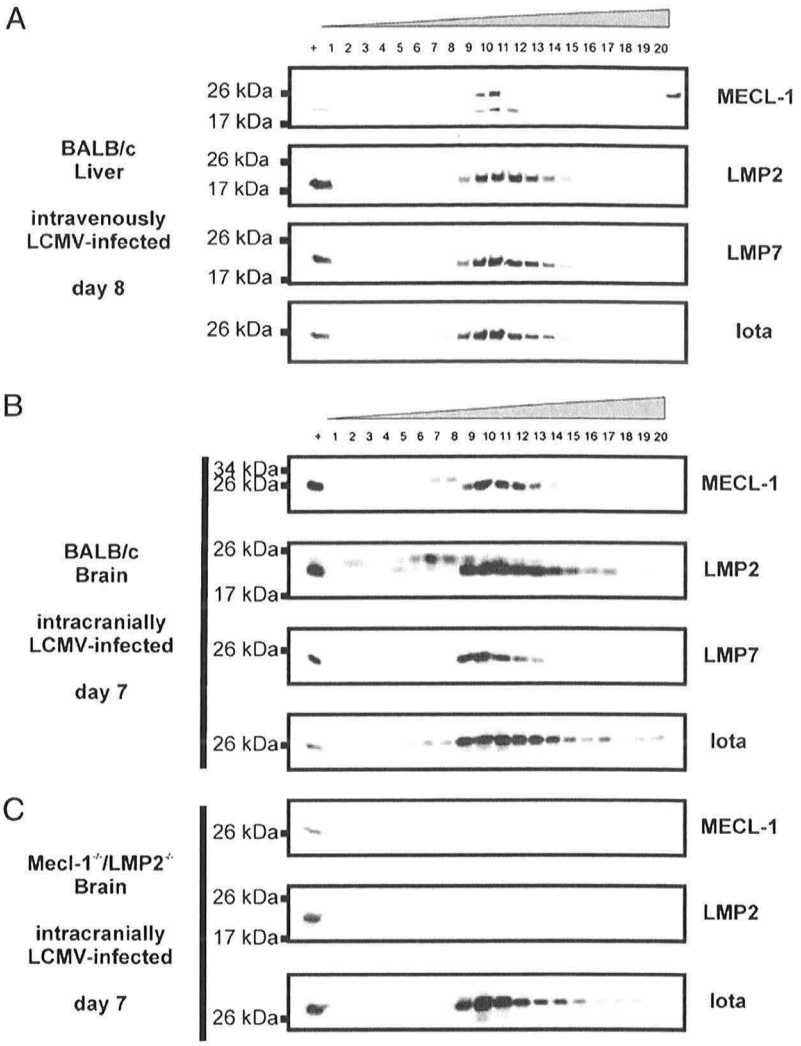

FIGURE 5. Analysis of mature immunoproteasome subunits and their precursors by density gradient centrifugation. Total lysates of liver and brain of LCMV-infected mice were directed to sucrose gradient ultracentrifugation. Immunoproteasome subunits within the respective fractions were detected by Western blot. As a positive control (+), purified immunoproteasome from a LCMV-infected BALB/c liver was loaded. The density increases from 15 to 40% toward fraction 20. Liver of mice infected i.v. with LCMV-WE on day 8 postinfection (*A*); brain of wild-type (*B*), and MECL-1$^{-/-}$/LMP2$^{-/-}$ double knockout (*C*) mice intracranially infected with LCMV-WE on day 7 postinfection. The experiments were performed three times with similar outcome.

fluorescence was detected in the meninges, the outer brain parenchyma, the ventricular ependymal cells, and the regions around the ventricles. At a higher magnification, LMP2^{+} cells in the ventricular region revealed a ramified morphology suggesting microglia as potential producers of immunoproteasome.

Colocalization of LMP2/MECL-1 and Iba-1 in the brains of LCMV-infected mice

Next we investigated a possible localization of immunoproteasomes in microglia after intracranial LCMV infection. As a marker for microglia we used Iba-1, also named allograft inflammatory factor-1 (AIF-1). Iba-1 is exclusively expressed in cells of the monocytic lineage and is associated with microglial activation in the brain (30). Its constitutive expression prevails in CNS-associated macrophages in the perivascular space and the meninges as well as in microglia within the brain parenchyma. Most prominent signals for Iba-1 were observed in the region of the meningeal and ventricular regions with most prominent staining in the region around the 4th ventricle. Comparing naive mice with intracranially LCMV-infected mice, we observed a significant increase in the number of microglia and intensity of Iba-1 staining within these regions of infected mice (data not shown).

To investigate if microglia express immunoproteasomes in the LCMV-infected brain, wild-type mice as well as MECL-1$^{-/-}$/LMP2$^{-/-}$ knockout mice were infected with 30 PFU LCMV-WE intracranially. On day 7 postinfection, brains were recovered, and coronal cryosections of the diencephalon were costained for Iba-1 and LMP2 or MECL-1, respectively. As expected, MECL-1$^{-/-}$/LMP2$^{-/-}$ double-deficient mice showed no signal for both immunoproteasome subunits indicating the specificity of the immunoproteasome staining (Fig. 6*A*, 6*B*). Concerning the expression of LMP2 and MECL-1 in wild-type mice, we observed a partial colocalization with Iba-1, which was most prominent in the outer regions of the cerebral cortex in close proximity to the meninges, which persisted beyond day 10 postinfection (data not shown). Second-stage controls and compensation controls confirmed the specificity of stainings for LMP2, MECL-1, and Iba-1 (data not shown). We conclude that Iba-1^{+} cells are the main producers of immunoproteasome after intracranial LCMV infection. Although perivascular as well as meningeal macrophages and monocytes are also known to express Iba-1, the Iba-1^{+}LMP2^{+} cells as well as the Iba-1^{+}MECL-1^{+} cells can be assigned to be microglia due to their characteristic morphology. However, in addition, we also saw some immunoproteasome-positive cells that were Iba-1 negative.

After intracranial LCMV infection, immunoproteasome can be detected exclusively in the nuclei of astrocytes

Astrocytes represent the main glial cell type within the brain. They are involved in many processes related to CNS homeostasis

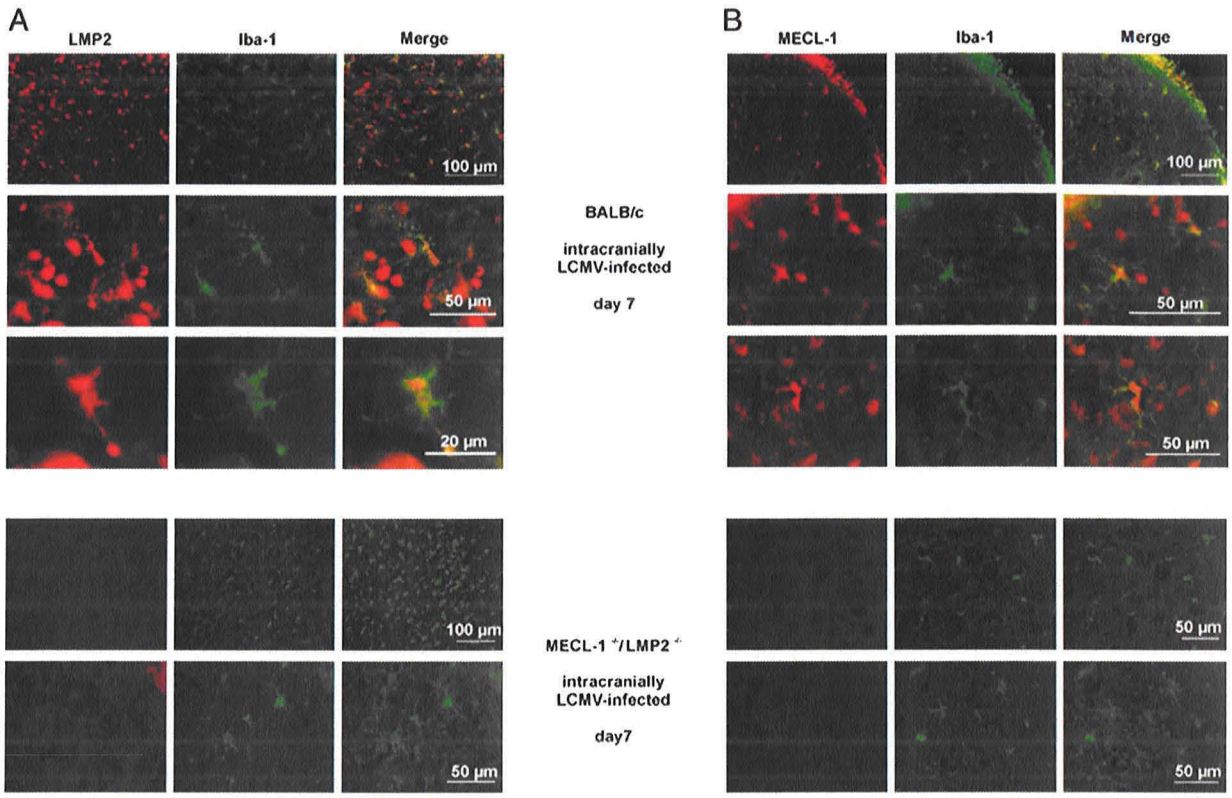

FIGURE 6. Colocalization of LMP2 and MECL-1 with the microglia marker Iba-1 in the brain of LCMV-infected BALB/c mice. Coronal brain cryosections of LCMV-infected BALB/c mice and MECL-1$^{-/-}$/LMP2$^{-/-}$ double knockout mice were costained for LMP2 or MECL-1, which was visualized using a cy3-coupled anti-rabbit Ab (red), and the microglial cell marker Iba-1, which was visualized using an Alexa 488-coupled anti-goat Ab (green). *A*, Costaining of LMP2 and Iba-1. *B*, Costaining of MECL-1 and Iba-1. The magnifications of shown images range from ×100 to ×400. The experiments were performed four times yielding similar images.

including the release of neurotrophic factors and the guidance of neuronal development, the regulation of extracellular pH and K^+ levels, and the formation and maintenance of the blood–brain barrier. After activation, astrocytes proliferate and enhance the expression of GFAP in a process termed astrogliosis, which represents a common feature of many neurodegenerative diseases (31). A comparison of naive versus LCMV-infected brain sections showed a slight increase in the number of stained astrocytes that was most obvious in the region of the 4th ventricle and the hippocampus (data not shown). We performed costainings for GFAP and LMP2 or MECL-1, respectively, of brain sections of BALB/c mice, which were intracranially infected with 30 PFU LCMV-WE alone or coinfected with 30 PFU intracranially and 10^5 PFU i.p. Second-stage and compensation controls confirmed the specificity of the GFAP stainings (Supplemental Fig. 3*B*, 3*C*). In contrast with microglia, we could not observe any colocalization of GFAP and immunoproteasome in the cytosol of astrocytes either on day 7 postinfection or on day 10 postinfection (Supplemental Fig. 3*A*). However, images of GFAP$^+$ astrocytes of higher magnification revealed LMP2 staining in astrocytes that did not colocalize with the intermediate filament GFAP in the cytosol but rather colocalized with DAPI in nuclei of GFAP$^+$ astrocytes (Fig. 7). MECL-1 also colocalized with DAPI in nuclei of GFAP$^+$ astrocytes (Supplemental Fig. 4), suggesting that astrocytes accumulate immunoproteasome in the nucleus.

Immunoproteasome cannot be detected in neurons and oligodendrocytes of LCMV-infected mouse brain

We also analyzed the capacity of neurons and oligodendrocytes to express immunoproteasome. As a marker for neurons, we used a mouse Ab that recognizes a neuron-specific nuclear protein called NeuN. Oligodendrocytes were detected using an Ab specific for 2′,3′-cyclic nucleotide 3′-phosphodiesterase (CNPase), which is a marker for oligodendrocytes and Schwann cells. Bleed-through and second-stage controls showed no unspecific staining for both cell types (Supplemental Fig. 5*C*). The analysis of the coexpression of LMP2 and NeuN revealed that the majority of neurons did not express immunoproteasome (Supplemental Fig. 5*A*), although a few neuronal nuclei in areas of strong immunoproteasome expression appeared to be slightly positive for LMP2. In costainings of LMP2 and CNPase, we failed to detect any colocalization indicating that oligodendrocytes do not express immunoproteasomes (Supplemental Fig. 5*B*).

Immunoproteasome expression in isolated microglial cell populations

To corroborate further our immunohistochemical data testifying to immunoproteasome formation in microglia, we determined the immunoproteasome expression in CD11b$^+$ cells magnetically sorted from single-cell suspensions of intracranially LCMV-infected brains by Western blot analysis (Fig. 8). The quality of the isolation was analyzed by flow cytometric analysis and revealed purities of the isolated CD11b$^+$ cells between 75 and 90% (data not shown). The immunoproteasome subunits LMP2 and LMP7 were exclusively found in isolated CD11b$^+$ cells, whereas expression of the α-subunit iota, which is present in constitutive and immunoproteasome, could also be detected in the flow-through fraction indicating the expression of constitutive proteasome in other cell types of the brain. Taken together, these data confirm microglia, macrophages, or perhaps neutrophils as the

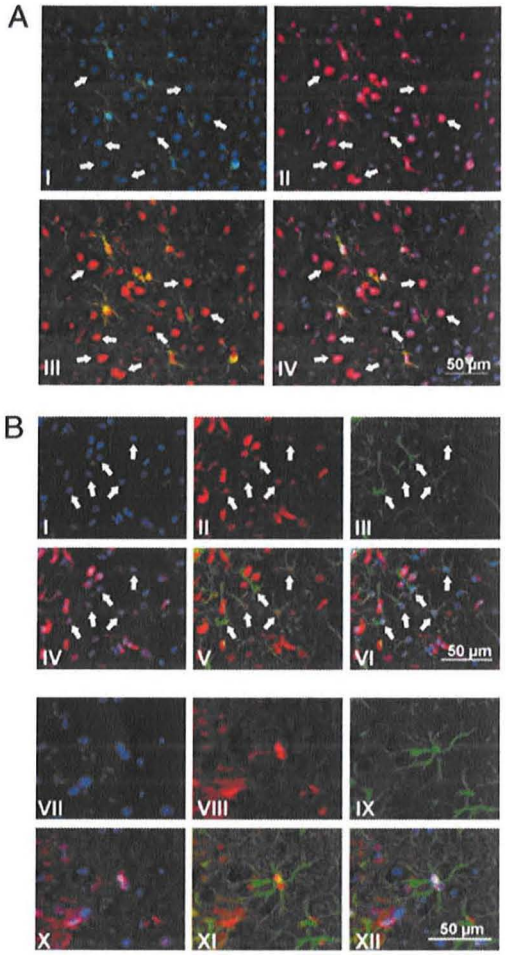

FIGURE 7. *A*, LMP2 colocalizes with DAPI in the nuclei of non-microglia cells. Cryosections of intracranially LCMV-infected BALB/c mice on day 7 postinfection were immuno-histochemically stained for Iba-1 (green), LMP2 (red), and DAPI (blue). (*I*) DAPI + Iba-1. (*II*) DAPI + LMP2. (*III*) LMP2 + Iba-1. (*IV*) DAPI + LMP2 + Iba-1. White arrows indicate cell nuclei, which are positive for LMP2 and not related to microglia cells. *B*, Localization of LMP2 in the nuclei of astrocytes. Brain cryosections of LCMV-infected BALB/c mice were stained for LMP2 (red) and GFAP (green). Nuclei were counterstained with DAPI. (*I*) DAPI alone. (*II*) LMP2 alone. (*III*) GFAP alone. (*IV*) DAPI + LMP2. (*V*) LMP2 + GFAP. (*VI*) DAPI + LMP2 + GFAP. The magnifications of shown images range from ×100 to ×400. The experiments were performed three times with similar outcomes.

main cell types expressing immunoproteasome in the brain after intracranial LCMV infection. Although immunoproteasome staining was observed in nuclei of astrocytes by immunohistology (Fig. 7, Supplemental Fig. 4), according to Western analysis (Fig. 8), CD11b$^-$ cells do not seem to contribute significantly to the total pool of immunoproteasome in the brain.

Immunoproteasome expression in astrocytes after in vitro stimulation with IFN-γ

To investigate further the immunoproteasome expression in astrocytes under inflammatory conditions, we decided to stimulate primary astrocytes with IFN-γ in vitro. Primary astrocytes, which were prepared from the cortices of neonatal BALB/c mice, were cultured for 3 wk and subsequently either left untreated or stimulated with 20 ng/ml IFN-γ for 72 h. Afterward, the immunoproteasome expression was analyzed in total lysates by Western

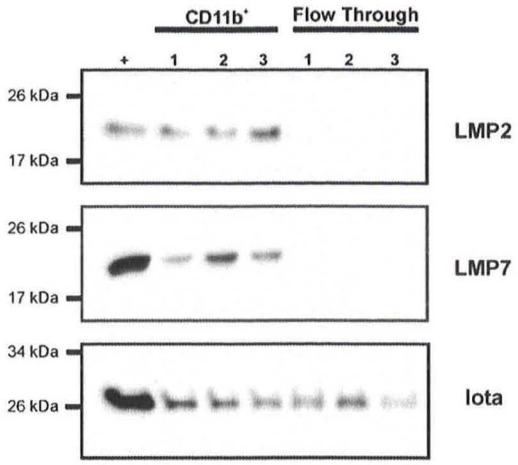

FIGURE 8. Immunoproteasome expression in isolated microglia. Three BALB/c mice were intracranially infected with 30 PFU LCMV-WE. On day 7 postinfection, single-cell suspensions were generated from the brains and CD11b$^+$ cells isolated by magnetic sorting. After the purity of the isolated fractions has been confirmed by flow cytometry, total lysates of the fractions were analyzed for their immunoproteasome content by Western blot using Abs specific for LMP2, LMP7, and the constitutive α-type proteasome subunit iota (α1). As a positive control (+), purified immunoproteasome from LCMV-infected mouse liver was used. The experiment was reproduced two times.

blot for LMP2, LMP7, and MECL-1. As shown in Fig. 9, primary astrocytes expressed matured LMP2 and LMP7 exclusively after stimulation with IFN-γ. Notably, the protein band detected in astrocytes with the MECL-1–specific Ab showed a molecular mass of ~30 kDa, which was significantly higher than that of

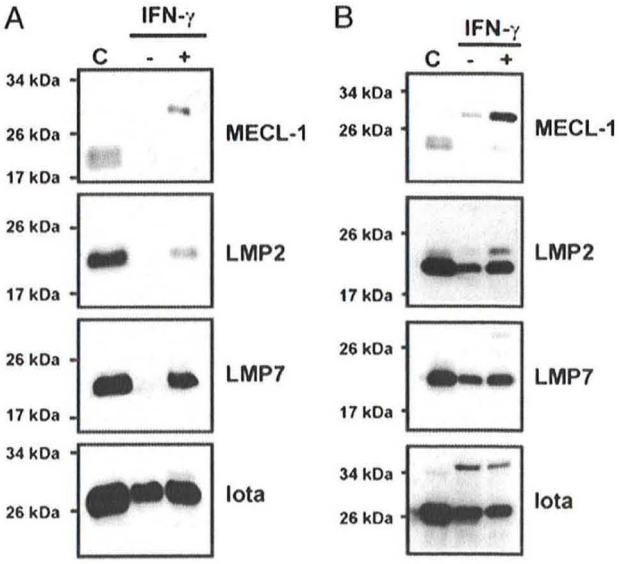

FIGURE 9. Immunoproteasome expression in primary and immortalized astrocyte cultures after IFN-γ stimulation. Primary astrocyte cultures were generated from neonatal BALB/c mice. After 3 wk in culture, cells were either left untreated or stimulated for 72 h in the presence of 20 ng/ml IFN-γ. In addition, immortalized astrocytes were either left untreated or stimulated with 20 ng/ml IFN-γ for 72 h. Total lysates from (*A*) primary astrocyte cultures or (*B*) immortalized astrocytes were analyzed by Western blot for the expression of MECL-1, LMP2, LMP7, and Iota. As a positive control, C, purified immunoproteasome from LCMV-infected mouse liver was used. The experiments were performed twice and yielded similar results.

mature MECL-1 in highly purified mouse 20S immunoproteasomes with a size of 25 kDa, suggesting that primary astrocytes contain the MECL-1 precursor but not the mature subunit. We also analyzed the immunoproteasome expression in an immortalized astrocytic cell line. In immortalized astrocytes, we observed expression of mature LMP7 and LMP2 in the presence and absence of IFN-γ but also detected an accumulation of LMP2 (23 kDa) and MECL-1 (30 kDa) precursors after IFN-γ stimulation (Fig. 9*B*). The immortalized astrocyte line showed low immunoproteasome expression of both mature and immature subunits already in unstimulated cells, suggesting that they had partially lost their inducibility. These data suggest that the observed accumulation of unprocessed, immunoproteasome precursors in the brain of intracranially LCMV-infected mice occurs in astrocytes, whereas microglia and monocytes, which represent the main producers of immunoproteasome, contain mainly mature immunoproteasome.

Immunoproteasomes contribute to the severity of LCMV-induced meningitis

Recently, a new function of immunoproteasomes in governing the production of proinflammatory cytokines and differentiation of Th17 cells has been described (1, 32). To assess whether immunoproteasomes may contribute to the immunopathological development of meningitis triggered by intracranial LCMV infection, we infected both C57BL/6 wild-type and LMP7$^{-/-}$ mice with LCMV-WE intracranially and monitored the meningitis disease score over time (Fig. 10). The onset of meningitis symptoms in LMP7$^{-/-}$ mice was delayed by 20 h (164 h compared with 144 h postinfection in wild-type mice), and the severity of disease was lower in LMP7-deficient mice at all time points. Moreover, wild-type mice had to be euthanized 164 h postinfection because of severe symptoms of meningitis, whereas LMP7$^{-/-}$ mice survived about 1 d longer. Given that LMP7 activity is required for the normal production of proinflammatory cytokines (32) and that microglia and macrophages, which produced these cytokines, are the only cell types in the inflamed CNS that assemble considerable amounts of mature immunoproteasomes, we propose that LMP7 deficiency might limit the inflammation-promoting function of these professional APCs in the CNS.

Discussion

The antiviral immune response leads to the production of the proinflammatory cytokines IFN-γ and TNF-α, which establish the inflammatory environment. One effect of these cytokines is a strong transcriptional induction of the immunoproteasome subunits LMP2 (β1i), MECL-1 (β2i), and LMP7 (β5i), which leads to the replacement of the constitutive subunits δ (β1), MC14 (β2), and MB1(β5) in the inflamed tissue. We analyzed the proteasome composition in different mouse organs after LCMV infection. We observed in most organs an extensive change from constitutively expressed proteasomes in a noninfected state toward immunoproteasomes in infected organs (Fig. 1). The brain, however, was different. Despite a cytokine-driven induction of immunoproteasome on the transcriptional level (Fig. 3), this induction resulted in only marginal replacement of constitutive proteasomes by immunoproteasomes on day 7 postinfection (Fig. 2).

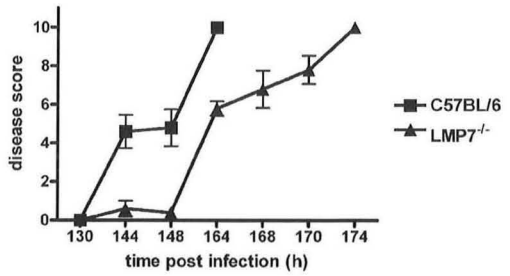

FIGURE 10. Delayed meningitis development in LMP7-deficient mice. C57BL/6 wild-type mice (squares) and LMP7$^{-/-}$ mice (triangles) were infected with 30 PFU LCMV-WE intracranially. Disease score (*y*-axis) was assessed as outlined in *Materials and Methods* and regularly graded in a blinded manner at indicated time intervals (in hours) postinfection. Data points represent mean ± SD of five mice. The experiments were performed twice and yielded similar results.

The assembly of the (immuno-)proteasome during neosynthesis is a multistep event, where N-terminal prosequences as well as carboxy-terminal extensions of the subunits actively participate in correct assembly leading to the autocatalytic cleavage of N-terminal prosequences and functional activation (7). While performing sucrose gradient centrifugation with brain lysates from LCMV-infected mice, we found an accumulation of immunoproteasome precursors (Fig. 5) in 16S gradient fractions suggesting that the dimerization of two half-proteasomes and autocatalytic processing of immunoproteasome subunits seems to be impeded in the brain. Although the mature forms of LMP2 and MECL-1 are predominant also in the LCMV-infected brain, the mere detection of LMP2 and MECL-1 precursors indicates that immunoproteasome assembly is impeded (8). The precursors are hardly detectable in Western analysis if immunoproteasomal precursor processing proceeds normally as precursor complexes are either rapidly matured or degraded if they fail to mature (33, 34). Based on these data, we postulate the existence of a posttranslational mechanism that regulates immunoproteasome formation in cells of the CNS, where no—or low—immunoproteasome expression is desired despite ongoing IFN release. This hypothesis is attractive given that the brain is an immune-privileged organ, where uncontrolled inflammatory responses may cause destruction of essential and poorly regenerating cells. To prevent immunopathologic damage, the unique anatomy of the brain including the blood–brain barrier and the blood–CSF barrier as well as the absence of classic lymphatic vessels clearly provides the cells of the CNS with a protective status against overt immune attack. However, in addition to these anatomic features, immune tolerance in the brain is also actively maintained by molecular determinants one of which may be the reduced formation of immunoproteasomes. The proteasome regulators PI31, PA200, PA28α, or the assembly factor UMP1, which all have been proposed to affect immunoproteasome assembly, were not significantly different in their expression in the intracranially infected brain compared with i.v. infected liver (A. Dahler, unpublished observations) and thus are not likely to play a role in the observed failure of proper immunoproteasome formation in the brain.

Despite major advances in proteasome research, the characterization of proteasome expression and activity in the CNS is still rudimentary. To get a deeper insight into immunoproteasome expression in the inflamed brain, we established an immunohistochemical protocol for the detection of immunoproteasome-expressing cells using Abs directed against peptide epitopes of mMECL-1 and mLMP2, which according to three-dimensional structure models should be accessible from the outer surface of the assembled immunoproteasome. This was an important prerequisite for this study as the 20S proteasome is very stable and not easily denatured by methods that should preserve the cellular structures in brain slices. The Abs used turned out to be excellently suited for the histological detection of immunoproteasome in brain cryosections. Moreover, they were able to detect the respective precursors pre–MECL-1 and pre-LMP2 in Western blots. We obtained specific stainings for the respective subunits in brain

cryosections of intracranially LCMV-infected mice that were absent in naive mice and in the respective LCMV-infected knockout mice underlining the reliability of the performed stainings (Supplemental Figs. 1, 2). Such important negative controls have not been applied in earlier immunohistochemical studies of immunoproteasome expression (35, 36) raising some doubts about the interpretation of these studies. Costainings with cell markers specific for neurons (NeuN) and oligodendrocytes (CNPase) showed no to low colocalization with the respective immunoproteasome subunits (Supplemental Fig. 5), indicating that these cells do no not seem to express immunoproteasome in vivo. Using Iba-1 as a marker specific for microglia cells, infiltrating monocytes, and macrophages, we could identify these cells as the main producers of immunoproteasome in the inflamed murine brain with strong immunoproteasome expression in the cytosol and the nucleus (Fig. 6). This confirms previous results by Stohwasser et al. (15) who could induce immunoproteasome expression in isolated microglia and the microglia cell line BV-2 upon stimulation with IFN-γ. Microglia are generally considered to be immunologically quiescent under nonpathological conditions as indicated by their ramified morphology, marginal expression of MHC class I molecules, and the complete absence of MHC class II surface expression. After activation, however, they transform into highly active effector cells as indicated by their contracted morphology and their proliferation. Due to an IFN-γ–induced increase in MHC class I and MHC class II surface expression, as well as the upregulation of costimulatory molecules such as B7.1 (CD80), B7.2 (CD86), and ICAM-1, they are the most-efficient APC population in the brain parenchyma (35, 37). Our finding that upon a viral infection these cells adapt their proteasome composition to the requirements of an optimized MHC class I epitope processing by the expression of immunoproteasome strongly supports this hypothesis and suggests that in the context of viral infection, these cells participate in Ag presentation. In contrast, the Ag presentation capacity of astrocytes, the major glial cell population, remains in question and is controversially discussed. Although increased astrocytic cell numbers are associated with many neurodegenerative diseases and could be shown to present myelin basic protein to encephalitogenic T cells (38), their presentation capacity remains a matter of debate. Sedgwick and colleagues (39) could show that astrocytes can activate T cells only if these cells were incubated in the presence of microglia or IL-1, indicating that an additional APC is required.

In this study, we hardly could observe any cytosolic expression of MECL-1 or LMP2 in $GFAP^+$ astrocytes (Supplemental Fig. 3), indicating that these cells do not seem to participate in the generation of immunoproteasome-dependent epitopes. Based on our immunohistochemical data, we therefore postulate that in the LCMV-infected brain, the function of Ag processing and presentation is mainly fulfilled by microglia, which represent the most dominant immunoproteasome-expressing cell population in the brain. An additional role of CNS-associated DCs and macrophages was not analyzed but cannot be excluded and seems to be quite likely, whereas neurons, oligodendrocytes, and astrocytes do not seem to be involved.

To investigate further the observed accumulation of immunoproteasome precursors in the brain of LCMV-infected mice, we analyzed the maturation status of immunoproteasomes expressed by microglia: $CD11b^+$ cells were isolated from LCMV-infected mouse brains, and total lysates were analyzed by Western blot. Both LMP2 and LMP7 were mature and fully processed suggesting proteolytic competence of immunoproteasomes in microglia (Fig. 8). In contrast, immunoproteasome expression was absent in the cytosol and instead MECL-1 and LMP2 were detected in the nuclei of astrocytes (Fig. 7, Supplemental Fig. 4). It remains to be investigated whether these nuclear immunoproteasomes are proteolytically active, mature immunoproteasomes or if they represent unprocessed, immature proteasome precursors that are deposited in the nucleus in an inactive state. The exclusive detection of MECL-1 precursors rather than mature MECL-1 in total lysates of IFN-γ–stimulated, primary astrocytes (Fig. 9) strongly suggest astrocytes as candidate cells accounting for the accumulation of immunoproteasomal precursors in brain and together with our in vivo histochemical data would be consistent with the involvement of the nuclear envelope in the compartmentalization of partially assembled immunoproteasomes. Enenkel and colleagues (40, 41) showed that in yeast, 13S–16S proteasome precursor complexes described as half-proteasomes are transported via karyopherin into the nucleus, and they postulated that in yeast the final dimerization step and the autocatalytic processing of β-subunits takes place in the nucleus. In case this finding would be extended to higher eukaryotes, the nuclear immunoproteasome staining in astrocytes may be due to an attenuation of nuclear proteasome assembly in astrocytes. Moreover, one could speculate on the presence of an additional factor facilitating proper immunoproteasome maturation and translocation back into the cytosol that is missing in activated astrocytes thus causing the accumulation of immunoproteasomes in the nucleus. To date, none of the described 20S proteasome assembly factors, the α-ring chaperone PAC1-4, and the β-ring chaperone hUMP1 show selectivity for immunoproteasomes compared with constitutive proteasomes. On the other hand, the multitude of recently discovered 26S proteasome chaperones should encourage the search for differently expressed immunoproteasome-selective assembly factors. It is quite striking that both in primary astrocytes and in one astrocytic cell line, IFN-γ–inducible MECL-1 precursors of 30 kDa accumulate in the absence of mature MECL-1 (25 kDa). Consistent with this accumulation, the LMP2 precursor (23 kDa) also accumulated in an immortalized astrocytic cell line upon IFN-γ induction, which may reflect the partial dependence of LMP2 processing on the presence of MECL-1 in the complex (8, 16). In primary astrocytes, no accumulation of LMP2 precursor was detected, but the quantity of mature LMP2 was very low compared with that of mature LMP7. LMP7 is known to incorporate into 20S proteasomes independently of LMP2 and MECL-1 and may hence not be affected by the accumulation of MECL-1 precursors.

Proteasome inhibition becomes an emerging strategy for the treatment of a variety of autoimmune, neurodegenerative, and proliferative disorders: bortezomib, a proteasome-specific inhibitor applied in the treatment of multiple myeloma, reduces cytokine production upon inflammation. However, its therapeutic suitability is limited due to considerable toxicities, and its therapeutic use in chronic inflammations remains problematic. Recently, Muchamuel et al. (32) presented an immunoproteasome-specific inhibitor targeting the chymotrypsin-like activity of the LMP7 subunit. In animal models of autoimmune disorders including diabetes and collagen-induced arthritis, PR-957 treatment afforded an impressive attenuation of disease and a suppression of proinflammatory cytokines (42). This novel function of immunoproteasomes might also explain why we could observe a protracted and less severe course of meningitis in $LMP7^{-/-}$ mice compared with that in C57BL/6 wild-type mice. Given that microglia-like cells seem to be the only cell types in the CNS that produce substantial amounts of intact immunoproteasomes, we assume that the lack of LMP7-dependent production of proinflammatory cytokines by these cells most likely accounts for the amelioration of LCMV-induced meningitis, which constitutes a new phenotype of $LMP7^{-/-}$ mice.

Understanding the role of immunoproteasome expression as well as the role of its reduced formation in the brain could provide new insights into how an immune response is regulated in an immune-privileged organ and how immune tolerance can be actively attained. Immunoproteasome-specific inhibitors like PR-957 will be instrumental in this respect and may represent a promising strategy for the treatment of chronic inflammation-associated neurologic disorders.

Acknowledgments

We thank Anja Dahler, Regina Preywisch, and Edward Málaga-Trillo for experimental support, and Ulrike Beck, Marianne Wiechers, and Ulrike Binkle for excellent technical assistance. Klaus Scherrer is acknowledged for generously providing the iota Ab, and Klaus Pfizenmaier for the contribution of immortalized astrocytes.

Disclosures

The authors have no financial conflicts of interest.

References

1. Groettrup, M., C. J. Kirk, and M. Basler. 2010. Proteasomes in immune cells: more than peptide producers? *Nat. Rev. Immunol.* 10: 73–78.
2. Groll, M., L. Ditzel, J. Löwe, D. Stock, M. Bochtler, H. D. Bartunik, and R. Huber. 1997. Structure of 20S proteasome from yeast at 2.4 A resolution. *Nature* 386: 463–471.
3. Aki, M., N. Shimbara, M. Takashina, K. Akiyama, S. Kagawa, T. Tamura, N. Tanahashi, T. Yoshimura, K. Tanaka, and A. Ichihara. 1994. Interferon-γ induces different subunit organizations and functional diversity of proteasomes. *J. Biochem.* 115: 257–269.
4. Groettrup, M., R. Kraft, S. Kostka, S. Standera, R. Stohwasser, and P.-M. Kloetzel. 1996. A third interferon-γ-induced subunit exchange in the 20S proteasome. *Eur. J. Immunol.* 26: 863–869.
5. Nandi, D., H. Jiang, and J. J. Monaco. 1996. Identification of MECL-1 (LMP-10) as the third IFN-γ-inducible proteasome subunit. *J. Immunol.* 156: 2361–2364.
6. Chen, P., and M. Hochstrasser. 1996. Autocatalytic subunit processing couples active site formation in the 20S proteasome to completion of assembly. *Cell* 86: 961–972.
7. Schmidtke, G., R. Kraft, S. Kostka, P. Henklein, C. Frömmel, J. Löwe, R. Huber, P. M. Kloetzel, and M. Schmidt. 1996. Analysis of mammalian 20S proteasome biogenesis: the maturation of beta-subunits is an ordered two-step mechanism involving autocatalysis. *EMBO J.* 15: 6887–6898.
8. De, M., K. Jayarapu, L. Elenich, J. J. Monaco, R. A. Colbert, and T. A. Griffin. 2003. Beta 2 subunit propeptides influence cooperative proteasome assembly. *J. Biol. Chem.* 278: 6153–6159.
9. Groettrup, M., M. van den Broek, K. Schwarz, A. Macagno, S. Khan, R. de Giuli, and G. Schmidtke. 2001. Structural plasticity of the proteasome and its function in antigen processing. *Crit. Rev. Immunol.* 21: 339–358.
10. Mishto, M., E. Bellavista, A. Santoro, A. Stolzing, C. Ligorio, B. Nacmias, L. Spazzafumo, M. Chiappelli, F. Licastro, S. Sorbi, et al. 2006. Immunoproteasome and LMP2 polymorphism in aged and Alzheimer's disease brains. *Neurobiol. Aging* 27: 54–66.
11. Ding, Q., and J. N. Keller. 2001. Proteasomes and proteasome inhibition in the central nervous system. *Free Radic. Biol. Med.* 31: 574–584.
12. Keller, J. N., F. F. Huang, and W. R. Markesbery. 2000. Decreased levels of proteasome activity and proteasome expression in aging spinal cord. *Neuroscience* 98: 149–156.
13. Piccinini, M., M. Mostert, S. Croce, S. Baldovino, M. Papotti, and M. T. Rinaudo. 2003. Interferon-gamma-inducible subunits are incorporated in human brain 20S proteasome. *J. Neuroimmunol.* 135: 135–140.
14. Díaz-Hernández, M., F. Hernández, E. Martín-Aparicio, P. Gómez-Ramos, M. A. Morán, J. G. Castaño, I. Ferrer, J. Avila, and J. J. Lucas. 2003. Neuronal induction of the immunoproteasome in Huntington's disease. *J. Neurosci.* 23: 11653–11661.
15. Stohwasser, R., J. Giesebrecht, R. Kraft, E. C. Müller, K. G. Häusler, H. Kettenmann, U. K. Hanisch, and P. M. Kloetzel. 2000. Biochemical analysis of proteasomes from mouse microglia: induction of immunoproteasomes by interferon-gamma and lipopolysaccharide. *Glia* 29: 355–365.
16. Basler, M., J. Moebius, L. Elenich, M. Groettrup, and J. J. Monaco. 2006. An altered T cell repertoire in MECL-1-deficient mice. *J. Immunol.* 176: 6665–6672.
17. Van Kaer, L., P. G. Ashton-Rickardt, M. Eichelberger, M. Gaczynska, K. Nagashima, K. L. Rock, A. L. Goldberg, P. C. Doherty, and S. Tonegawa. 1994. Altered peptidase and viral-specific T cell response in LMP2 mutant mice. *Immunity* 1: 533–541.
18. Fehling, H. J., W. Swat, C. Laplace, R. Kühn, K. Rajewsky, U. Müller, and H. von Boehmer. 1994. MHC class I expression in mice lacking the proteasome subunit LMP-7. *Science* 265: 1234–1237.
19. Khan, S., M. van den Broek, K. Schwarz, R. de Giuli, P. A. Diener, and M. Groettrup. 2001. Immunoproteasomes largely replace constitutive proteasomes during an antiviral and antibacterial immune response in the liver. *J. Immunol.* 167: 6859–6868.
20. Wessel, D., and U. I. Flügge. 1984. A method for the quantitative recovery of protein in dilute solution in the presence of detergents and lipids. *Anal. Biochem.* 138: 141–143.
21. Pfaffl, M. W., G. W. Horgan, and L. Dempfle. 2002. Relative expression software tool (REST) for group-wise comparison and statistical analysis of relative expression results in real-time PCR. *Nucleic Acids Res.* 30: e36.
22. Falsig, J., P. Pörzgen, J. Lotharius, and M. Leist. 2004. Specific modulation of astrocyte inflammation by inhibition of mixed lineage kinases with CEP-1347. *J. Immunol.* 173: 2762–2770.
23. Frisa, P. S., M. N. Goodman, G. M. Smith, J. Silver, and J. W. Jacobberger. 1994. Immortalization of immature and mature mouse astrocytes with SV40 T antigen. *J. Neurosci. Res.* 39: 47–56.
24. Langford, D. J., A. L. Bailey, M. L. Chanda, S. E. Clarke, T. E. Drummond, S. Echols, S. Glick, J. Ingrao, T. Klassen-Ross, M. L. Lacroix-Fralish, et al. 2010. Coding of facial expressions of pain in the laboratory mouse. *Nat. Methods* 7: 447–449.
25. Oehen, S., H. Hengartner, and R. M. Zinkernagel. 1991. Vaccination for disease. *Science* 251: 195–198.
26. Shin, E. C., U. Seifert, T. Kato, C. M. Rice, S. M. Feinstone, P. M. Kloetzel, and B. Rehermann. 2006. Virus-induced type I IFN stimulates generation of immunoproteasomes at the site of infection. *J. Clin. Invest.* 116: 3006–3014.
27. Campbell, I. L., M. V. Hobbs, P. Kemper, and M. B. A. Oldstone. 1994. Cerebral expression of multiple cytokine genes in mice with lymphocytic choriomeningitis. *J. Immunol.* 152: 716–723.
28. Groettrup, M., S. Standera, R. Stohwasser, and P. M. Kloetzel. 1997. The subunits MECL-1 and LMP2 are mutually required for incorporation into the 20S proteasome. *Proc. Natl. Acad. Sci. USA* 94: 8970–8975.
29. Kang, S. S., and D. B. McGavern. 2008. Lymphocytic choriomeningitis infection of the central nervous system. *Front. Biosci.* 13: 4529–4543.
30. Ito, D., Y. Imai, K. Ohsawa, K. Nakajima, Y. Fukuuchi, and S. Kohsaka. 1998. Microglia-specific localisation of a novel calcium binding protein, Iba1. *Brain Res. Mol. Brain Res.* 57: 1–9.
31. Eng, L. F., and R. S. Ghirnikar. 1994. GFAP and astrogliosis. *Brain Pathol.* 4: 229–237.
32. Muchamuel, T., M. Basler, M. A. Aujay, E. Suzuki, K. W. Kalim, C. Lauer, C. Sylvain, E. R. Ring, J. Shields, J. Jiang, et al. 2009. A selective inhibitor of the immunoproteasome subunit LMP7 blocks cytokine production and attenuates progression of experimental arthritis. *Nat. Med.* 15: 781–787.
33. Schmidtke, G., M. Schmidt, and P. M. Kloetzel. 1997. Maturation of mammalian 20S proteasome: purification and characterization of 13S and 16S proteasome precursor complexes. *J. Mol. Biol.* 268: 95–106.
34. Murata, S., H. Yashiroda, and K. Tanaka. 2009. Molecular mechanisms of proteasome assembly. *Nat. Rev. Mol. Cell Biol.* 10: 104–115.
35. Ferrington, D. A., S. A. Hussong, H. Roehrich, R. J. Kapphahn, S. M. Kavanaugh, N. D. Heuss, and D. S. Gregerson. 2008. Immunoproteasome responds to injury in the retina and brain. *J. Neurochem.* 106: 158–169.
36. Egerer, T., L. Martinez-Gamboa, A. Dankof, B. Stuhlmüller, T. Dörner, V. Krenn, K. Egerer, P. E. Rudolph, G. R. Burmester, and E. Feist. 2006. Tissue-specific up-regulation of the proteasome subunit beta5i (LMP7) in Sjögren's syndrome. *Arthritis Rheum.* 54: 1501–1508.
37. Frei, K., C. Siepl, P. Groscurth, S. Bodmer, C. Schwerdel, and A. Fontana. 1987. Antigen presentation and tumor cytotoxicity by interferon-gamma-treated microglial cells. *Eur. J. Immunol.* 17: 1271–1278.
38. Fontana, A., W. Fierz, and H. Wekerle. 1984. Astrocytes present myelin basic protein to encephalitogenic T-cell lines. *Nature* 307: 273–276.
39. Sedgwick, J. D., R. Mössner, S. Schwender, and V. ter Meulen. 1991. Major histocompatibility complex-expressing nonhematopoietic astroglial cells prime only CD8+ T lymphocytes: astroglial cells as perpetuators but not initiators of CD4+ T cell responses in the central nervous system. *J. Exp. Med.* 173: 1235–1246.
40. Lehmann, A., K. Janek, B. Braun, P. M. Kloetzel, and C. Enenkel. 2002. 20 S proteasomes are imported as precursor complexes into the nucleus of yeast. *J. Mol. Biol.* 317: 401–413.
41. Wendler, P., A. Lehmann, K. Janek, S. Baumgart, and C. Enenkel. 2004. The bipartite nuclear localization sequence of Rpn2 is required for nuclear import of proteasomal base complexes via karyopherin alphabeta and proteasome functions. *J. Biol. Chem.* 279: 37751–37762.
42. Basler, M., M. Dajee, C. Moll, M. Groettrup, and C. J. Kirk. 2010. Prevention of experimental colitis by a selective inhibitor of the immunoproteasome. *J. Immunol.* 185: 634–641.